

Article

CNT-TiO_{2-δ} Composites for Improved Co-Catalyst Dispersion and Stabilized Photocatalytic Hydrogen Production

Peirong Chen ^{1,†,*}, Lidong Wang ², Ping Wang ¹, Aleksander Kostka ³, Michael Wark ^{1,4}, Martin Muhler ¹ and Radim Beranek ^{2,*}

¹ Laboratory of Industrial Chemistry, Ruhr-University Bochum, Universitätsstrasse 150, 44780 Bochum, Germany; E-Mails: wp198558@gmail.com (P.W.); michael.wark@uni-oldenburg.de (M.W.); muhler@techem.ruhr-uni-bochum.de (M.M.)

² Inorganic Chemistry, Ruhr-University Bochum, Universitätsstrasse 150, 44780 Bochum, Germany; E-Mail: lidong.wang@rub.de

³ Department of Microstructure Physics and Alloy Design, Max-Planck-Institut für Eisenforschung, Max-Planck-Strasse 1, 40237 Düsseldorf, Germany; E-Mail: a.kostka@mpie.de

⁴ Institute of Chemistry, Carl von Ossietzky University Oldenburg, Carl-von-Ossietzky-Str. 9-11, 26129 Oldenburg, Germany

† Present address: Institute of Inorganic Chemistry, RWTH Aachen University, Landoltweg 1, 52074 Aachen, Germany.

* Authors to whom correspondence should be addressed; E-Mails: peirongc@outlook.com (P.C.); radim.beranek@rub.de (R.B.); Tel.: +49-234-32-29431 (R.B.) Fax: +49-234-32-14174 (R.B.).

Academic Editor: Bunsho Ohtani

Received: 19 December 2014 / Accepted: 23 February 2015 / Published: 2 March 2015

Abstract: Composites consisting of carbon nanotubes (CNTs) grown directly on oxygen-deficient anatase TiO₂ (TiO_{2-δ}) were synthesized by a two-step chemical vapor deposition (CVD) method and applied in photocatalytic hydrogen production from aqueous methanol solutions using photodeposited Pt as the co-catalyst. Thermogravimetry coupled with mass spectroscopy, X-ray diffraction, scanning electron microscopy, photocurrent analysis, X-ray photoelectron spectroscopy, and (scanning) transmission electron microscopy were performed to investigate the physical and (photo)chemical properties of the synthesized CNT-TiO_{2-δ} composites before and after photocatalytic methanol reforming. The initial photocatalytic activity of TiO₂ was found to be significantly improved in the presence of oxygen vacancies. An optimized amount (~7.2 wt%) of CNTs

grown on the $\text{TiO}_{2-\delta}$ surface led to a highly effective stabilization of the photocatalytic performance of $\text{TiO}_{2-\delta}$, which is attributed to the improved dispersion and stability of the photodeposited Pt co-catalyst nanoparticles and enhanced separation efficiency of photogenerated electron-hole pairs, rendering the photocatalysts less prone to deactivation.

Keywords: carbon nanotubes; TiO_2 ; oxygen deficiency; photocatalytic hydrogen production; platinum co-catalyst; stability

1. Introduction

Photocatalytic production of hydrogen by water splitting is considered to be a promising route toward efficient conversion of solar energy [1,2]. One of the key issues in solar water-splitting is the development of efficient and stable systems for light-driven reduction of protons to hydrogen. Among other materials, titanium dioxide (TiO_2) is comprehensively studied as a photocatalyst for hydrogen production due to its relatively negative position in the conduction band edge allowing for proton reduction, low cost, high stability and the possibility of further functionalization [3–8].

One of the commonly observed and applied features for TiO_2 is that its activity can be significantly enhanced by surface and/or bulk defects resulting from, for example, the introduction of heteroatoms or the removal of lattice oxygen [3,4,6]. Doping with metallic (Nb, Ag, Pt, W, Mn, *etc.*) and/or non-metallic (C, N, P, F, *etc.*) heteroatoms has been proven to be one effective route and is thus widely used in practice [9–12]. Recently, hydrogenation, *i.e.*, reduction in hydrogen, was found to be another efficient route to create defects and to obtain oxygen-deficient TiO_2 ($\text{TiO}_{2-\delta}$) [6,13]. As compared to the doping method, hydrogenation of TiO_2 seems to be more promising due to its high efficiency and easy operation. For example, in photodegradation reactions, significantly higher activity can be achieved over $\text{TiO}_{2-\delta}$ than pristine TiO_2 [5,6,8]. In photocatalytic water splitting, the efficiency of $\text{TiO}_{2-\delta}$ is rather moderate [14], and further improvement of the activity and stability is required.

Compositing TiO_2 with carbon nanomaterials, such as carbon nanotubes (CNTs) and graphene [15,16], was reported to be an effective tool for enhancing the efficiency of the separation of photogenerated electron-hole (e^- - h^+) pairs because of the excellent electric conductivity of carbon nanomaterials, which resulted in more active and more stable photocatalyst for dye degradation and water splitting [15–19]. Nevertheless, most of the preparation of carbon- TiO_2 composites was in the context of physical mixing, either in solution [18,19] or via mechanical routes [20], and thus, the photocatalytic performance of TiO_2 was only limitedly improved due to the insufficient electronic contact between the TiO_2 and the carbon nanoparticles. Therefore, in order to further increase the photocatalytic performance, it is necessary to improve the junction quality between carbon nanomaterials and TiO_2 , which requires more delicately designed preparation strategies.

In this work, a two-step chemical vapor deposition (CVD) approach was applied in the synthesis of CNT- $\text{TiO}_{2-\delta}$ composites [21]. As compared to those prepared by physical mixing [18–20], composites in this work consist of CNTs grown directly on anatase TiO_2 particles and are able to significantly improve the electronic contact between the CNTs and TiO_2 particles [21]. Furthermore, the oxygen deficiency of TiO_2 , which is created prior to and during the CNT synthesis under reducing atmosphere,

can contribute to the separation of photogenerated e^-h^+ pairs. As a result, the CNT-TiO_{2-δ} composite synthesized under optimal conditions displayed significantly improved performance stability in the photocatalytic production of hydrogen from aqueous methanol solutions.

2. Results and Discussion

2.1. Physicochemical Properties

The time for the CVD growth of CNTs was varied from 5 min to 60 min in order to obtain different carbon contents on TiO_{2-δ}. The synthesized CNT-TiO_{2-δ} composites with a growth time of 5, 15 and 60 min were denoted as CNT-TiO_{2-δ}-5, CNT-TiO_{2-δ}-15 and CNT-TiO_{2-δ}-60, respectively. In the case of CNT growth with a shorter time than 60 min, additional treatment in He was performed, aiming at an identical duration of 60 min at 550 °C for all of the samples. The applied reducing atmosphere prior to and during the CNT growth is known to form oxygen-deficient TiO_{2-δ} [21]. For comparison, pristine TiO₂ was subjected to the same preparation procedure, except that C₂H₄ in the CNT growth step was replaced by He. The resulting sample was designated as TiO_{2-δ}.

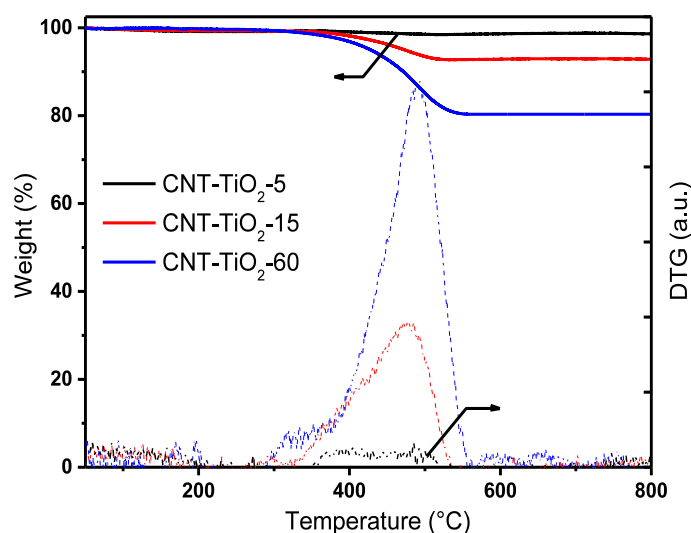


Figure 1. TG (solid lines) and DTG (dashed lines) curves for the CNT-TiO_{2-δ} composites. Black: CNT-TiO_{2-δ}-5 (5, five minutes); red: CNT-TiO_{2-δ}-15; blue: CNT-TiO_{2-δ}-60.

To determine the amount and the thermal stability of CNTs synthesized by the method used, TG analysis in synthetic air was performed with the obtained CNT-TiO_{2-δ} composites. The TG and differential TG (DTG) curves for the CNT-TiO_{2-δ} composites are shown in Figure 1. It can be seen that the weight loss of the CNT-TiO_{2-δ}-15 and CNT-TiO_{2-δ}-60 composites mainly occurred in the temperature range between 400 and 550 °C (Figure 1), which is characteristic for the combustion of CNTs in air [22]. Correspondingly, DTG curves that are typical for CNT combustion were observed for these CNT-TiO_{2-δ} composites, as well. No significant weight loss was detected at temperatures above 550 °C, indicating the complete total oxidation of CNTs at lower temperatures. The main DTG peak was found to be at much lower temperatures for CNT-TiO_{2-δ}-5 than the other CNT-TiO_{2-δ}

composites, which is attributed to the presence of poorly crystallized carbon, e.g., amorphous carbon and carbon deposition due to the incomplete decomposition of C_2H_4 on the $TiO_{2-\delta}$ surface [23].

CNT contents of the CNT- $TiO_{2-\delta}$ composites were determined based on the calibrated weight loss, and the results are summarized in Table 1. It can be seen that the CNT content in the CNT- $TiO_{2-\delta}$ composites increased with growth time, which is also reflected in the DTG curves (Figure 1) and the mass spectrometry (MS) profiles of m/z 44 corresponding to CO_2 resulting from the CNT combustion (Figure S1).

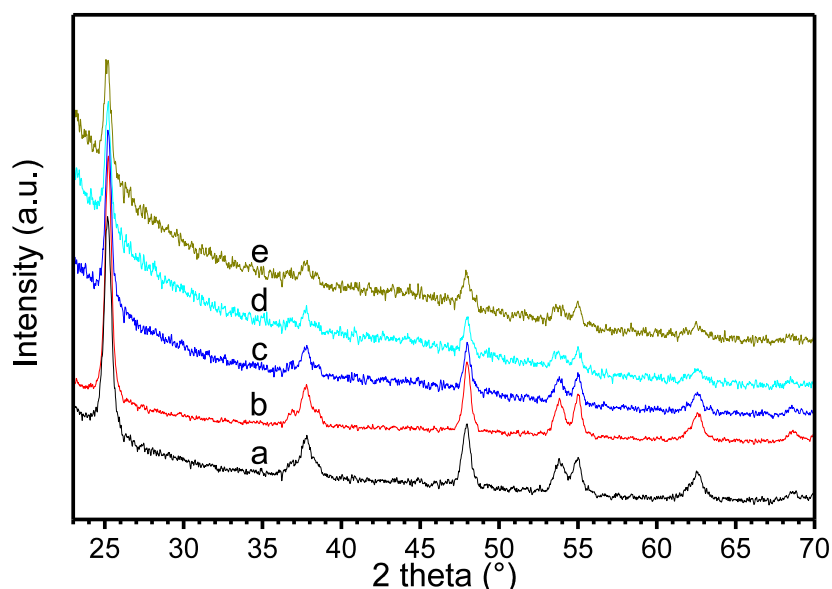


Figure 2. XRD patterns of pristine TiO_2 (a), $TiO_{2-\delta}$ (b), CNT- $TiO_{2-\delta-5}$ (c), CNT- $TiO_{2-\delta-15}$ (d) and CNT- $TiO_{2-\delta-60}$ (e).

Table 1. CNT contents (derived from the weight loss in TG analysis), BET surface areas and the average H_2 evolution rates (with Pt co-catalyst) before and after resuming the reaction (r_1 and r_2).

Catalyst	C (wt%)	BET ($m^2 g^{-1}$)	r_1 ($mmol h^{-1}$)	r_2 ($mmol h^{-1}$)
Pristine TiO_2	-	104	13.4	4.2
$TiO_{2-\delta}$	-	92	18.2	6.2
CNT- $TiO_{2-\delta-5}$	1.4	73	8.2	2.6
CNT- $TiO_{2-\delta-15}$	7.2	79	9.7	8.1
CNT- $TiO_{2-\delta-60}$	19.3	71	6.8	6.5

The BET surface areas of pristine TiO_2 , $TiO_{2-\delta}$ and the CNT- $TiO_{2-\delta}$ composites are summarized in Table 1. $TiO_{2-\delta}$ and the CNT- $TiO_{2-\delta}$ composites show clearly lower BET surface areas than the pristine TiO_2 , due to the agglomeration of TiO_2 particles at high temperatures [21]. However, no significant difference of particle size was observed between TiO_2 and $TiO_{2-\delta}$ by SEM (Figure S2), indicating that the agglomeration was limited to a small extent. In the CNT- $TiO_{2-\delta}$ composites, the covering of TiO_2 by CNTs leads to an additional loss of accessible surface area. XRD patterns shown in Figure 2 revealed that the pure anatase phase is present in oxygen-deficient $TiO_{2-\delta}$ and all of the CNT- $TiO_{2-\delta}$ composites [24]. Clear CNT diffraction peaks were not observed in any of the

CNT-TiO_{2-δ} composites, probably due to the insufficiently crystalline structure of the CNTs synthesized at relatively low temperature.

SEM images in Figure 3 show the morphologies of the CNT-TiO_{2-δ} composites with varied growth time. It can be seen that CNTs were hardly detected in CNT-TiO_{2-δ}-5 (Figure 3A). Well-defined CNTs can be clearly observed on TiO_{2-δ} by extending the growth time to 15 min (CNT-TiO_{2-δ}-15, Figure 3B), whereas a growth time of 60 min (CNT-TiO_{2-δ}-60) led to TiO_{2-δ} fully covered by CNTs, as shown in Figure 3C. Although the length of CNTs in CNT-TiO_{2-δ}-60 is significantly greater than that in CNT-TiO_{2-δ}-15, due to a longer growth time, all of the observed CNTs have a diameter of around 40–50 nm and were homogeneously grown on the surface of the TiO_{2-δ} particles. It is supposed that the TiO₂ particles are also bridged by CNTs in the micro-scale range [25], because uniformly distributed Fe nanoparticles (indicated by the absence of clear FeO_x reflections in the XRD pattern of CVD-synthesized FeO_x/TiO₂ catalyst in Figure S3) serving as the catalyst for CNT growth form on the surface of TiO₂ [21,26]. As a consequence, a different performance from that of TiO₂ and TiO_{2-δ} can be expected for the CNT-TiO_{2-δ} composites in photocatalysis.

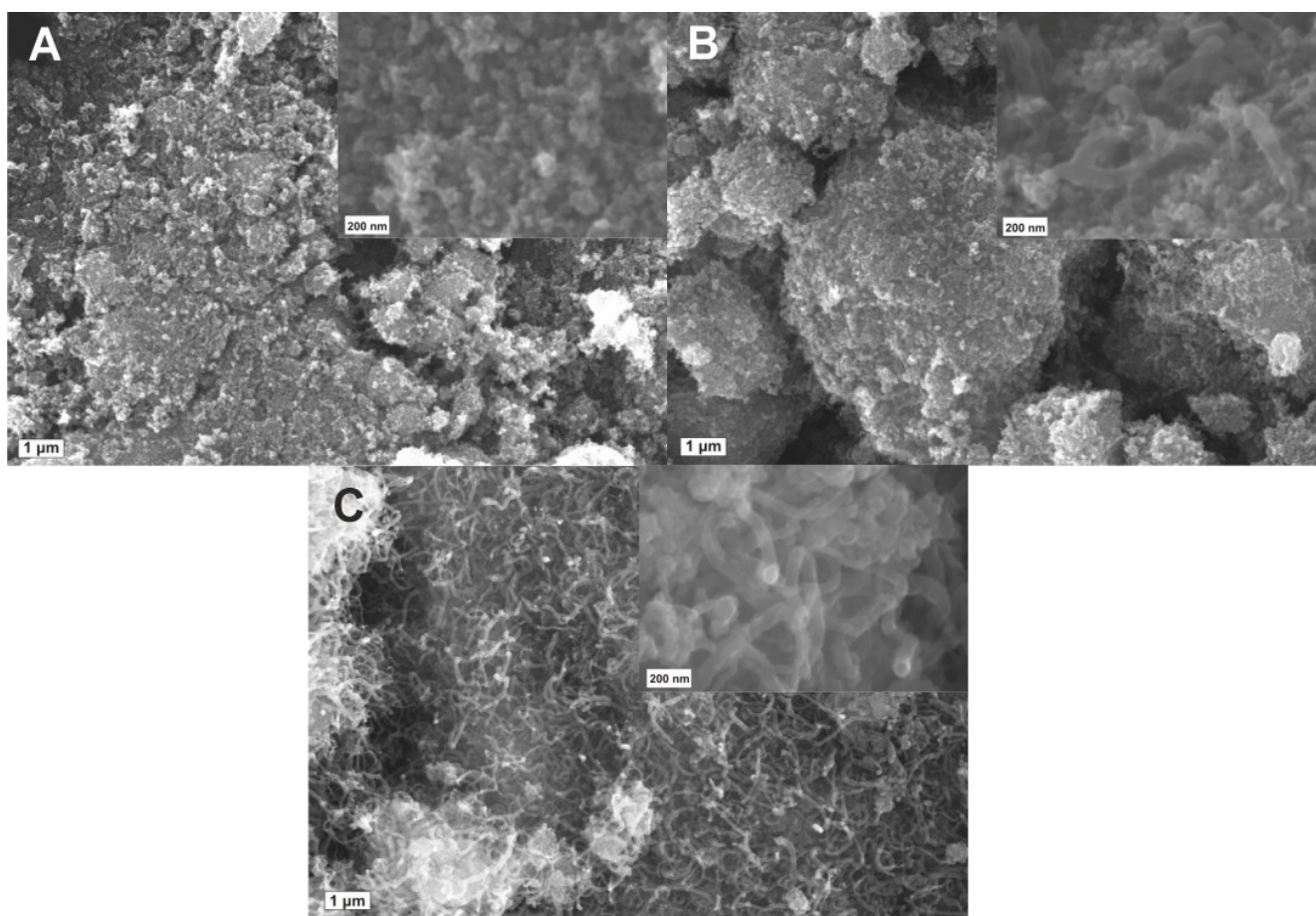
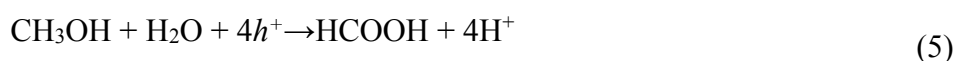
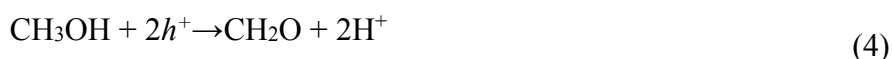


Figure 3. SEM images for CNT-TiO_{2-δ} composites with a growth time of 5 min (A), 15 min (B) and 60 min (C). The inserted images were taken at a higher magnification.

2.2. Photocatalytic Performance

The activities of CNT-TiO_{2-δ} composites were tested in the photocatalytic production of hydrogen from aqueous methanol solutions. Pristine TiO₂ and TiO_{2-δ} were examined for comparison. In the presence of photocatalysts with Pt co-catalyst, the following reactions can occur in the photocatalytic system [27,28]:



Notably, Reaction 6 (injection of the second electron, from the methoxy radical formed upon one-hole oxidation of methanol, into the conduction band of TiO₂) is likely to occur in our system, as corroborated by the photocurrent multiplication effect observed upon the addition of methanol (see Figure S2).

In the control experiments (Figure S4), only a negligible amount of H₂ (with a H₂ evolution rate smaller than 0.002 mmol h⁻¹) was evolved under UV illumination in pure water, and the addition of methanol into the reaction system did not essentially increase the H₂ evolution rates (remaining smaller than 0.5 mmol h⁻¹). Subsequently, Pt was deposited under UV irradiation following the protocol by Ohtani and coworkers using H₂PtCl₆ as the precursor [29,30]. It was confirmed that the complete photoreduction of the precursor to the metallic state and thorough deposition onto the catalyst surface occur in a short time [30], which is corroborated in this work by the short induction period (less than 5 min) for all of the tested catalysts (Figure 4). Afterwards, drastically enhanced H₂ evolution was observed for the photocatalysts used, demonstrating the importance of co-catalyst in this reaction. The amounts of evolved H₂ for pristine TiO₂, TiO_{2-δ} and all of the CNT-TiO_{2-δ} composites with Pt co-catalyst are displayed as a function of time (the Pt precursor was added into the reaction system at Time 0) in Figure 4.

In the first hour, the pristine TiO₂ showed high activity in terms of evolved H₂, and the introduction of oxygen deficiency further improved the hydrogen productivity of TiO₂ (Figure 4 and Figure S4) [6,13]. However, both the pristine TiO₂ and the TiO_{2-δ} photocatalysts were deactivated rapidly (Figure S4), probably due to the build-up of surface contaminants from the reaction, blocking the photoabsorption. In contrast, CNT-TiO_{2-δ}-15 and CNT-TiO_{2-δ}-60 as photocatalysts have clearly lower initial activities, but much higher stabilities in photocatalytic H₂ production (Figure 4 and Figure S4). On the one hand, the presence of CNTs leads to poorer photoabsorption of TiO_{2-δ} due to partial blocking of UV light by CNTs, as indicated by the lowered incident photon-to-current efficiency (IPCE) in Figure S5, and consequently lower overall photocatalytic activity of CNT-TiO_{2-δ}

composites, especially for CNT-TiO_{2-δ}-60 [19]. On the other hand, the presence of CNTs facilitates the separation of photogenerated e^-h^+ pairs in TiO_{2-δ} [17], which prohibits the oxidation of active oxygen-deficient Ti species and consequently leads to higher stability [15,31]. The CNT-TiO_{2-δ}-5 composite, however, showed no substantial improvement in terms of hydrogen productivity, probably due to the presence of a relatively large amount of poorly crystallized carbon (Figure 1) on the surface of TiO_{2-δ}, deteriorating the IPCE (Figure S5) [20].

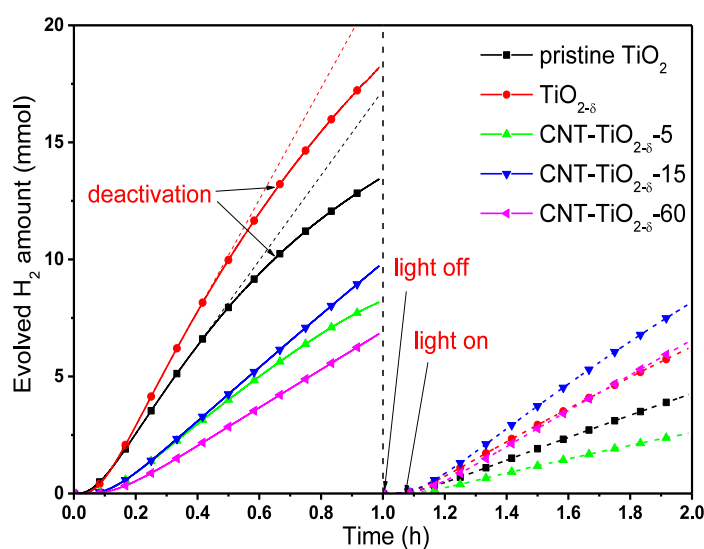


Figure 4. Evolved H₂ amount as a function of reaction time for different photocatalysts in photocatalytic hydrogen production. The reactions were carried out in aqueous methanol solutions (50 mL methanol in 500 mL pure water) using 0.2 g catalyst (pristine TiO₂, TiO_{2-δ} or CNT-TiO_{2-δ} composites). Before the reaction, 0.1 wt% Pt was photodeposited on the photocatalyst as the co-catalyst. The irradiation lamp was switched off after 1 h, and the reactor was purged with Ar for *ca.* 5 min to remove all of the evolved gaseous species. Then, the reaction was resumed, and the evolved H₂ amount was re-measured.

After resuming the reactions, lower activities in terms of H₂ productivity were observed for all the photocatalysts, which can be ascribed to the adsorbed intermediates of methanol reforming, blocking the surface active sites at TiO₂ or TiO_{2-δ} (see the discussion below) [28,32]. Nevertheless, a nearly linear accumulation of H₂ was achieved over all of the photocatalysts, indicating more stable photocatalytic performance. As compared to the pristine TiO₂, TiO_{2-δ} still demonstrated a higher activity, implying the importance of oxygen deficiency in this reaction [4,5]. Most importantly, CNT-TiO_{2-δ}-15 and CNT-TiO_{2-δ}-60 showed even higher H₂ productivity than TiO_{2-δ}. By comparing the average H₂ evolution rates before and after resuming the reaction (r_1 and r_2 values in Table 1, respectively), we notice a decrease of activity by *ca.* 65% for TiO_{2-δ}, whereas there is only a decrease by *ca.* 15% for CNT-TiO_{2-δ}-15 and less than 5% for CNT-TiO_{2-δ}-60. This observation clearly proves the beneficial effect of CNTs on the stability of photocatalytic performance and suggests that the presence of CNTs allows for efficient hydrogen evolution, even in the presence of surface contamination by carbon-containing reaction intermediates and products (see Reactions 1–6 above). Similar to the reaction before resuming, the highest photocatalytic activity was observed over

CNT-TiO_{2-δ}-15 among the three composites, whereas a detrimental influence resulting from poorly crystallized carbon or excess CNTs on TiO_{2-δ} was observed, as shown by the slower H₂ accumulation trends (Figure 4) and average H₂ evolution rates (*r*₂ values in Table 1) for CNT-TiO_{2-δ}-5 and CNT-TiO_{2-δ}-60. As a preliminary conclusion, the results imply that high-performance CNT-TiO_{2-δ} composites for photocatalytic hydrogen production can be obtained by delicately controlling the content of CNTs on the TiO_{2-δ} surface, in which a balance is achieved between two factors related to the presence of CNTs: the improved charge separation and stability and the diminished light absorption.

It is worth mentioning that the doping effect of Fe, as reported in the literature [33,34], is not possible in the CNT-TiO_{2-δ} composites, because the temperature used for the preparation and treatment of Fe/TiO₂ is not high enough to achieve the diffusion of Fe into the TiO₂ bulk [35]. In addition, the growth catalyst particles remaining in CNTs after purification are typically covered by several carbon layers and, therefore, separated from the TiO₂ particles [22,36,37].

2.3. XPS and (S)TEM of the Photocatalysts after Reactions

In order to gain further insight into the factors governing the photoactivity of our samples, after photocatalytic reactions, the surface chemistry of three representative photocatalysts, *i.e.*, TiO_{2-δ}, CNT-TiO_{2-δ}-15 and CNT-TiO_{2-δ}-60, was examined by XPS. In all three samples, Ti, O, C and Pt were detected. Both the Ti 2p and O 1s spectra were found to be in typical binding energy positions for TiO₂ and without a clear shift between samples (Figure 5A,B), indicating that CNTs on the surface did not change the chemical environment of Ti and O. Nevertheless, their intensities varied significantly between different samples, that is, the Ti 2p and O 1s for CNT-TiO_{2-δ}-60 photocatalyst have clearly lower intensities than the corresponding ones for the TiO_{2-δ} and CNT-TiO_{2-δ}-15 photocatalyst, which is due to the presence of CNTs covering the TiO_{2-δ} particles. Oxygen-deficient Ti species, *e.g.*, Ti³⁺, were not detected in any of the samples, presumably due to the very low amount and the complexity of the photocatalysts (*e.g.*, the presence of adsorbed intermediate species on the surface).

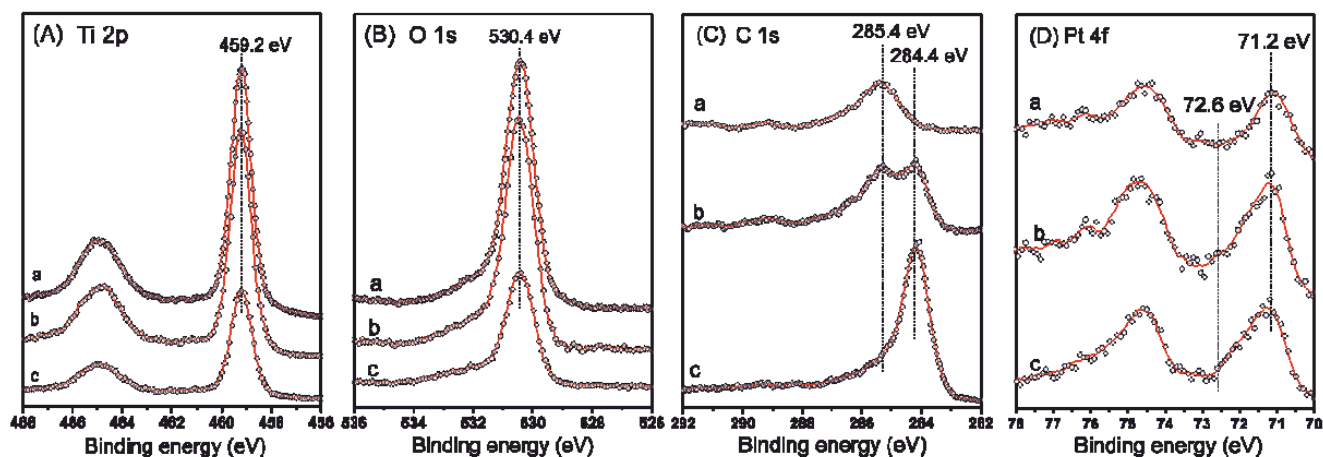


Figure 5. XP Ti 2p (A), O 1s (B), C 1s (C) and Pt 4f (D) spectra for TiO_{2-δ} (a), CNT-TiO_{2-δ}-15 (b) and CNT-TiO_{2-δ}-60 (c) with photodeposited Pt (0.1 wt%) after photocatalytic reactions.

Table 2. Surface compositions (in atomic percent, at%) of the photocatalysts after reactions derived from the quantitative XPS studies. Platinum (0.1 wt%) was photodeposited as the co-catalyst.

Catalyst	C	O	Ti	Pt
TiO _{2-δ}	20.34	55.03	24.47	0.16
CNT-TiO _{2-δ} -15	31.94	47.22	20.52	0.32
CNT-TiO _{2-δ} -60	54.81	32.08	12.76	0.35

Both the intensity and binding energy positions of C 1s spectra were found to vary significantly between different samples (Figure 5C). A major contribution at 285.4 eV was observed in the C 1s spectrum of the TiO_{2-δ} photocatalyst, mainly due to the carbon contamination during the storage and transfer of the samples upon contact with air. However, a minor contribution of the adsorbed carbon species from the photocatalytic reaction in aqueous methanol solution cannot be fully excluded [38]. Similar surface carbon content was observed for pristine TiO₂ photocatalyst by XPS (Figure S6 and Table S1). In the case of the CNT-TiO_{2-δ}-15 photocatalyst, in addition to the contribution at 285.4 eV, a second peak positioning at 284.4 eV was observed, as well, and is characteristic for carbon in CNTs [22], which led to an overall double-peak C 1s spectrum. A more intense C 1s spectrum with a shifted peak center at *ca.* 284.4 eV was recorded for CNT-TiO_{2-δ}-60, indicating that CNTs are the predominant carbon species. The major 4f_{7/2} peaks for Pt in all three samples were found to be at 71.2 eV and attributed to Pt in the metallic state (Figure 5D), indicating a complete photoreduction of the Pt precursor [22]. A much lower Pt intensity was observed on TiO_{2-δ} than on the two CNT-TiO_{2-δ}-based photocatalysts, which can be ascribed to the covering of Pt nanoparticles by very fine titania particles, being less visible in the surface-sensitive XPS measurements. The relatively more severe agglomeration of Pt nanoparticles on TiO_{2-δ} than on CNT-TiO_{2-δ} composites is believed to be responsible for the lower Pt intensity.

Quantitative analysis of the XPS spectra yielded surface compositions for the three photocatalysts as summarized in Table 2. As compared to TiO_{2-δ}, a significantly higher amount of carbon was found on the surface of CNT-TiO_{2-δ} photocatalysts, obviously due to the grown CNTs. Increasing the CNT growth time led to the increase of surface carbon content and, meanwhile, the decrease of surface O and Ti contents, implying that the TiO_{2-δ} surface was more completely covered, which is in accordance with the SEM results (Figure 3). Notably, significantly higher Pt contents were observed on CNT-TiO_{2-δ} composites than on TiO_{2-δ}, demonstrating the advantage of CNT-TiO_{2-δ} composites as a support for photodeposited Pt nanoparticles [22]. Obviously, the amount and morphology of Pt nanoparticles and their coupling with the light-absorbing TiO_{2-δ} plays a crucial role in photocatalytic hydrogen evolution, particularly in the presence of surface contamination by reaction intermediates/products. Therefore, a closer analysis of the size and distribution of the Pt nanoparticles was carried out.

STEM and TEM analysis revealed that the photodeposited Pt nanoparticles were dispersed uniformly on the surface of TiO_{2-δ} and CNT-TiO_{2-δ}-15 (Figures 6A,B and S7), whereas Pt nanoparticles on CNT-TiO_{2-δ}-60 were observed to agglomerate more severely (Figures 6C and S8). A statistical analysis of particle size was conducted over the TiO_{2-δ} and CNT-TiO_{2-δ}-15 photocatalysts by measuring the size of *ca.* 100 Pt nanoparticles in representative TEM images, and the histograms

yielded are shown in Figure 6D. It can be seen that a relatively smaller mean particle size with a narrower size distribution was obtained for Pt nanoparticles on CNT-TiO_{2-δ}-15 than on TiO_{2-δ}, showing the relevance of the presence of CNTs, which is in agreement with the higher surface concentration of Pt on CNT-TiO_{2-δ}-15 than on TiO_{2-δ}, as demonstrated by the quantitative XPS analysis (Table 2).

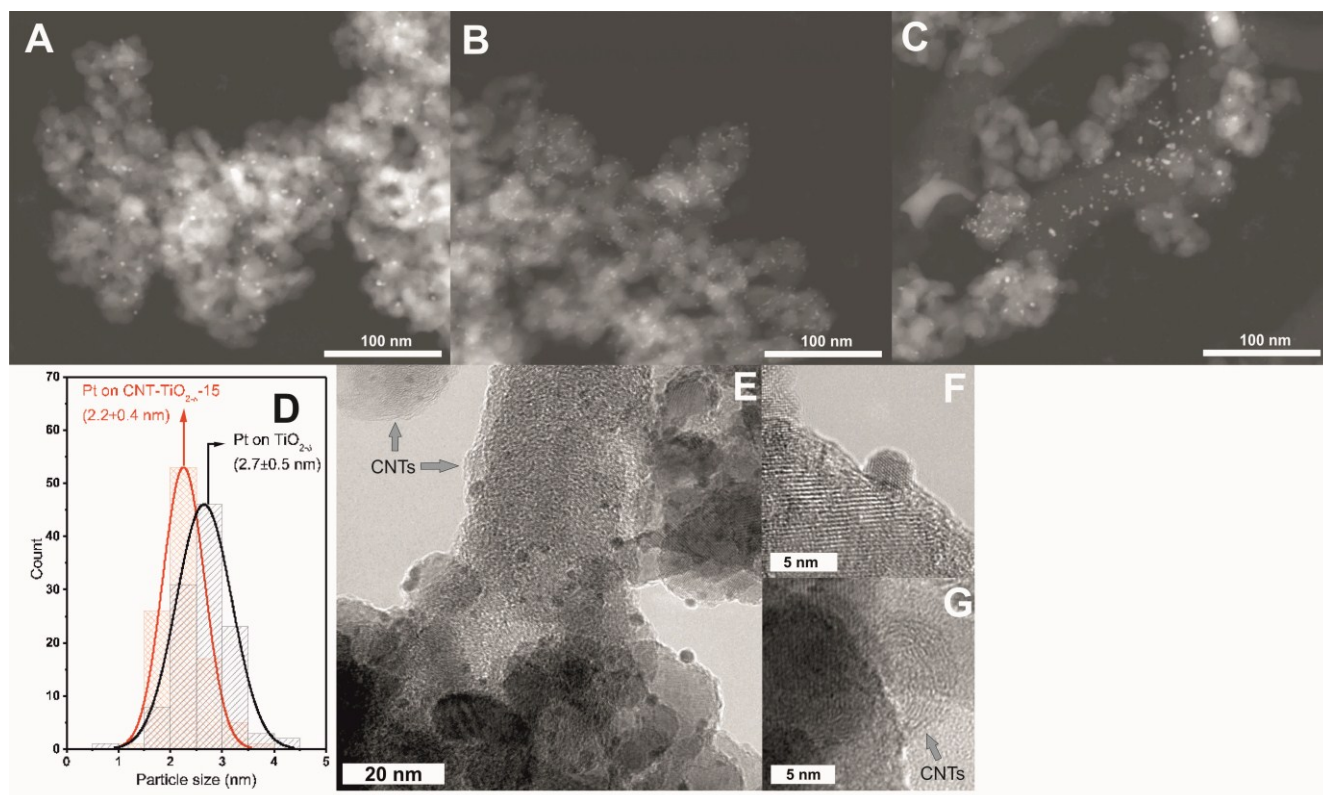


Figure 6. Representative STEM images for TiO_{2-δ} (A), CNT-TiO_{2-δ}-15 (B) and CNT-TiO_{2-δ}-60 (C) with photodeposited Pt nanoparticles and after photocatalytic reactions; particle size distributions of the Pt nanoparticles on CNT-TiO_{2-δ}-15 and on TiO_{2-δ} (D); TEM image of the CNT-TiO_{2-δ}-15 with photodeposited Pt nanoparticles (E); HRTEM image of Pt nanoparticle on CNT-TiO_{2-δ}-15 (F); HRTEM image of well-structured CNTs bridging two TiO_{2-δ} particles in CNT-TiO_{2-δ}-15 (G).

The TEM image in Figure 6E shows that Pt nanoparticles in the CNT-TiO_{2-δ}-15 photocatalyst are dispersed on both TiO_{2-δ} particles and CNTs without significant preference. The high-resolution TEM (HRTEM) image in Figure 6F shows the typical morphology of a Pt nanoparticle. Well-formed CNTs connecting the TiO_{2-δ} particles were also detected in the TEM analysis (Figures 6E and G). A poorly crystalline structure was observed in CNTs with a larger diameter and greater length (Figure 6E), whereas a highly crystalline structure was formed for CNTs with a shorter length and smaller diameters (Figure 6E,G). The latter is supposed to play a vital role in the transfer and separation of photogenerated e^-h^+ pairs [15,17,31].

According to the STEM and TEM results for CNT-TiO_{2-δ}-60, it is clear that increasing the growth time led to the formation of longer and large-diameter CNTs, which had a negative influence on the dispersion of the photodeposited Pt nanoparticles (Figures 6C and S8). Specifically, Pt nanoparticles

form larger agglomerates on the long and large-diameter CNTs far from $\text{TiO}_{2-\delta}$ particles. A large amount of surface defects on these less crystalline CNTs [39], which act as strong anchoring sites for Pt nanoparticles [22], was suggested to be the reason. This is in agreement with the fact that a higher surface Pt concentration was detected on CNT- $\text{TiO}_{2-\delta}$ -60 by XPS (Figure 5B and Table 2) in spite of a more severe particle agglomeration (Figure 6C). Nevertheless, these Pt nanoparticles on the long and large-diameter CNTs are supposed to contribute negligibly in photocatalytic reactions. On the one hand, the size of the CNTs prohibits the intimate contact between Pt nanoparticles and the neighboring $\text{TiO}_{2-\delta}$ particles serving as photocatalytically active sites. On the other hand, the long and large-diameter CNTs with poor crystallinity (Figure S8) are not expected to efficiently collect and transfer the photogenerated electrons [15,17,31], which impairs the subsequent functioning of Pt nanoparticles as co-catalyst to a large extent [40]. As a consequence, significantly lower activity in photocatalytic hydrogen production was observed for CNT- $\text{TiO}_{2-\delta}$ -60 than for CNT- $\text{TiO}_{2-\delta}$ -15 (Figure 4), in which the good crystallinity of CNTs and the optimized distribution of Pt nanoparticles yielded composite photocatalysts with optimized electron transfer to hydrogen-evolving surface catalytic sites on Pt, enhancing thusly the charge separation and rendering the photocatalyst less prone to deactivation due to the presence of methanol decomposition products.

3. Experimental Section

3.1. Materials and Sample Preparation

Commercial anatase TiO_2 (Sachtleben Chemie) with a specific surface area of *ca.* $100 \text{ m}^2 \text{ g}^{-1}$ was used as the starting material. The CNT- $\text{TiO}_{2-\delta}$ composites were obtained via a two-step CVD method, which was described elsewhere [21]. Iron oxide (with a nominal Fe loading of 2 wt%) supported on TiO_2 was synthesized in a vertically positioned CVD reactor using ferrocene (Merck, 98%) as the Fe precursor [41]. Reduction of the obtained $\text{FeO}_x/\text{TiO}_2$ composites was performed at $550 \text{ }^\circ\text{C}$ in flowing H_2 (50 vol% H_2 in He, 100 mL min^{-1}) to obtain metallic Fe and $\text{TiO}_{2-\delta}$ simultaneously. At the same temperature, CVD growth of CNTs was subsequently carried out using the supported Fe as the catalyst and a mixture of C_2H_4 and H_2 (57 vol% C_2H_4 , 43 vol% H_2 , 100 mL min^{-1}) as the gas feed [23]. The growth time was varied from 5 to 60 min in order to obtain different carbon contents on $\text{TiO}_{2-\delta}$. Prior to any further use, the synthesized CNT- $\text{TiO}_{2-\delta}$ composites were purified by washing in diluted HNO_3 solution [22].

3.2. Physicochemical Characterization

Static N_2 physisorption experiments were performed in a Quantachrome Autosorb-1-MP setup. Samples were degassed at $200 \text{ }^\circ\text{C}$ for 2 h before the measurements. The adsorption-desorption isotherm data were recorded in the relative pressure range of 0.05–1. The specific surface area was calculated according to the BET equation, assuming that the area covered by one N_2 molecule is 0.162 nm^2 . Thermogravimetric (TG) analysis was performed in synthetic air (20.5 vol% O_2 in N_2) using a Cahn TG 2131 thermobalance in order to examine both the thermal stability and the achieved amount of the synthesized carbon on $\text{TiO}_{2-\delta}$. The samples were heated up to $800 \text{ }^\circ\text{C}$ at a ramp of $2 \text{ }^\circ\text{C min}^{-1}$. The evolved gas species resulting from the carbon combustion were monitored by a coupled mass

spectrometer in the exhaust stream. The calibrated weight loss was used to determine the carbon content of each CNT-TiO_{2-δ} composite.

X-ray diffraction was measured using a PANalytical MPD diffractometer equipped with Cu K α radiation, a secondary graphite monochromator and 0.04 rad incident/secondary beam Soller slits. Measurement conditions were 45 kV, 40 mA, 0.5° divergence slit and 0.2-mm receiving slit width. A step width of 0.015° and 20-s scanning time were applied in all of the measurements. A high-resolution thermal field emission scanning electron microscope (SEM, Zeiss, LEO 1530 Gemini) was used to investigate the morphology of the CNT-TiO_{2-δ} samples. The SEM images were acquired using an acceleration voltage of 20 kV. Transmission electron microscopy (TEM) and scanning TEM (STEM) measurements were carried out with a Jeol JEM-2200FS instrument operated at 200 kV. The specimens for TEM and STEM were prepared by ultrasonically dispersing the powder samples in ethanol and dropping the suspension on a carbon-coated Au grid.

X-ray photoelectron spectroscopy (XPS) measurements were performed in an ultrahigh vacuum setup equipped with a high resolution Gammadata Scienta SES 2002 analyzer and a monochromatic Al K α X-ray source (1486.6 eV, operated at 14.1 kV and 30 mA). The spectra were acquired at 200 eV pass energy (high pass energy mode) at a pressure of 3.5 to 6 $\times 10^{-10}$ mbar. Charging effects during the measurements were mediated by applying a flood gun (SPECS). The CASA XPS program was employed in the analysis of XP spectra. Calibration of the measured data was performed by positioning the main Ti 2p peak at 459.2 eV for TiO₂. Quantitative analysis was performed based on the C 1s, O 1s, Ti 2p and Pt 4f spectra after Shirley background subtraction and by taking the atomic sensitivity factor (ASF) of each element into account, which is consistent with our previous work [22].

3.3. Photocatalytic and Photoelectrochemical Measurements

Photocatalytic hydrogen production was performed in a double-walled inner irradiation-type quartz reactor connected to a closed gas circulation system. The reaction temperature was maintained at 10 °C with a double-walled quartz jacket filled with a flow of cooling water from a thermostat (Lauda) to prevent any thermal effect. A 350-W Hg mid-pressure immersion lamp (Peschl UV-Consulting, 700 W, operated at 50% power) was used as the light source for irradiation. Argon was used as the carrier gas, and a continuous flow of 50 mL min⁻¹ was applied. The evolved gas mixture was analyzed using an online multi-channel analyzer (Emerson) equipped with a thermal conductivity detector for hydrogen. In a typical run, 0.2 g of photocatalyst (TiO₂, TiO_{2-δ} or CNT-TiO_{2-δ} composites) powders were added and suspended in aqueous methanol solution (50 mL of methanol in 500 mL of pure water), where methanol was acting as a sacrificial reagent for H₂ production. Before irradiation, the whole system, including the photocatalyst, was rinsed with Ar to completely remove dissolved air. Afterwards, Pt (a nominal loading of 0.1 wt%) as the co-catalyst was loaded onto the photocatalysts by *in situ* photoreduction of the H₂PtCl₆ precursor (0.42 mg), and the photocatalytic methanol reforming was initiated by switching on the UV lamp. After 1 h of reaction, the irradiation lamp was switched off, and the reactor was purged with Ar. The complete removal of all of the evolved gaseous species was indicated by the detector signal down to the baseline level. Then, the reaction was resumed by switching on the UV lamp, and the evolved H₂ amount was re-measured. Control experiments were

performed in either pure water or a water-methanol mixture under UV irradiation and in the presence of photocatalysts (*i.e.*, pristine TiO₂, TiO_{2-δ} or CNT-TiO_{2-δ}-60) without Pt co-catalyst.

The protocol for the preparation of electrodes for photocurrent measurements was described elsewhere [42]. Briefly, a suspension containing 100 mg of powder sample in 1 mL of ethanol was sonicated for 15 min and then evenly deposited onto ITO glass by doctor blading using scotch tape as the frame and spacer. The electrode was then dried at 80 °C, pressed for 3 min at a pressure of 200 kg cm⁻² and heated in flowing He (100 mL min⁻¹) at 400 °C for 60 min in order to achieve a good contact. The photoelectrochemical setup for photocurrent measurements consisted of a SP-300 BioLogic potentiostat and a three-electrode cell using a Pt counter electrode and an Ag/AgCl reference electrode. The photoelectrodes were pressed against an O-ring of the cell, leaving an irradiated area of 0.5 cm². The electrodes were irradiated from the backside (through the ITO glass) using a tunable monochromatic light source (Instytut Fotonowy) equipped with a 150-W Xenon lamp and a grating monochromator with a bandwidth of *ca.* 10 nm. Appropriate cut-off filters were used in order to eliminate second-order diffraction radiation. The photocurrent was firstly recorded in a phosphate buffer (pH 7.0) at 0.5 V *vs.* Ag/AgCl. The measurements were repeated after the addition of 2 mL methanol, and the corresponding IPCE (incident photon-to-current efficiency) values were calculated for each sample.

4. Conclusions

CNT-TiO_{2-δ} composites consisting of CNTs directly grown on TiO_{2-δ}, *i.e.*, oxygen-deficient TiO₂, were successfully synthesized via a two-step CVD method. The amount of CNTs can be precisely controlled by varying the growth time. CNTs were found to be uniformly grown on the surface of TiO_{2-δ} particles without altering the crystalline structure.

In the photocatalytic production of hydrogen using Pt as the co-catalyst, TiO_{2-δ} showed a significantly higher activity than pristine TiO₂, due to the presence of oxygen vacancies, but strongly deactivated in the absence of CNTs. In contrast, a certain amount of CNTs can effectively stabilize the photocatalytic activity of TiO_{2-δ} due to the beneficial effects of CNTs on the separation of photogenerated *e*⁻-*h*⁺ pairs and on the dispersion and anchoring of photodeposited Pt nanoparticles acting as co-catalyst. An excess amount of CNTs was found to deteriorate the activity of TiO_{2-δ}, which is attributed to the blocking of light absorption by CNTs fully covering the surface of TiO_{2-δ} and to the agglomeration of the photodeposited Pt nanoparticles at long and large CNTs. While attempts to enhance the initial photocatalytic activity of hydrogen evolving systems are indispensable, the present study highlights the crucial importance of functional stability as a key factor in the development of viable solar hydrogen production schemes and demonstrates that CNT-TiO_{2-δ} composite photocatalysts with high performance stability can be obtained by growing short and small-diameter CNTs on the surface of TiO_{2-δ}.

Acknowledgments

Financial support by the MIWFT-NRW within the project “Anorganische Nanomaterialien für Anwendungen in der Photokatalyse: Wasseraufbereitung und Wasserstoffgewinnung” and by the EU-FP7 Grant “4G-PHOTOCAT” (Grant No. 309636) is gratefully acknowledged. The authors thank

Wei Xia for fruitful discussions. P.W. acknowledges the support from the China Scholarship Council for a PhD scholarship.

Author Contributions

P.C., M.M., M.W., and RB developed the project and designed the experiments. P.C. synthesized the photocatalysts. P.C., L.W., P.W., and A.K. performed the measurements. All authors contributed to the manuscript preparation, and approved the final version of the manuscript.

Conflicts of Interest

The authors declare no conflicts of interest.

References

1. Ibhaddon, A.O.; Fitzpatrick, P. Heterogeneous photocatalysis: Recent advances and applications. *Catalysts* **2013**, *3*, 189–218.
2. Martin, D.J.; Reardon, P.J.; Moniz, S.J.; Tang, J. Visible light-driven pure water splitting by a nature-inspired organic semiconductor-based system. *J. Am. Chem. Soc.* **2014**, *136*, 12568–12571.
3. Park, J.H.; Kim, S.; Bard, A.J. Novel carbon-doped TiO₂ nanotube arrays with high aspect ratios for efficient solar water splitting. *Nano. Lett.* **2006**, *6*, 24–28.
4. Lo, H.-H.; Gopal, N.O.; Ke, S.-C. Origin of photoactivity of oxygen-deficient TiO₂ under visible light. *Appl. Phys. Lett.* **2009**, *95*, 83126–83128.
5. Chen, Y.; Cao, X.; Lin, B.; Gao, B. Origin of the visible-light photoactivity of NH₃-treated TiO₂: Effect of nitrogen doping and oxygen vacancies. *Appl. Surf. Sci.* **2013**, *264*, 845–852.
6. Leshuk, T.; Parviz, R.; Everett, P.; Krishnakumar, H.; Varin, R.A.; Gu, F. Photocatalytic activity of hydrogenated TiO₂. *ACS Appl. Mater. Interfaces* **2013**, *5*, 1892–1895.
7. Dozzi, M.V.; Selli, E. Specific facets-dominated anatase TiO₂: Fluorine-mediated synthesis and photoactivity. *Catalysts* **2013**, *3*, 455–485.
8. Wei, W.; Yaru, N.; Chunhua, L.; Zhongzi, X. Hydrogenation of TiO₂ nanosheets with exposed {001} facets for enhanced photocatalytic activity. *RSC Adv.* **2012**, *2*, 8286.
9. Mei, B.; Sánchez, M.D.; Reinecke, T.; Kaluza, S.; Xia, W.; Muhler, M. The synthesis of Nb-doped TiO₂ nanoparticles by spray drying: An efficient and scalable method. *J. Mater. Chem.* **2011**, *21*, 11781–11790.
10. Jin, Q.L.; Arimoto, H.; Fujishima, M.; Tada, H. Manganese oxide-surface modified titanium(IV) dioxide as environmental catalyst. *Catalysts* **2013**, *3*, 444–454.
11. Choi, J.; Park, H.; Hoffmann, M.R. Effects of single metal-ion doping on the visible-light photoreactivity of TiO₂. *J. Phys. Chem. C* **2010**, *114*, 783–792.
12. Liu, G.; Wang, L.; Yang, H.G.; Cheng, H.-M.; Lu, G.Q. Titania-based photocatalysts—Crystal growth, doping and heterostructuring. *J. Mater. Chem.* **2010**, *20*, 831–843.
13. Chen, X.; Liu, L.; Yu, P.Y.; Mao, S.S. Increasing solar absorption for photocatalysis with black hydrogenated titanium dioxide nanocrystals. *Science* **2011**, *331*, 746–750.

14. Zuo, F.; Wang, L.; Wu, T.; Zhang, Z.; Borchardt, D.; Feng, P. Self-doped Ti³⁺ enhanced photocatalyst for hydrogen production under visible light. *J. Amer. Chem. Soc.* **2010**, *132*, 11856–11857.
15. Leary, R.; Westwood, A. Carbonaceous nanomaterials for the enhancement of TiO₂ photocatalysis. *Carbon* **2011**, *49*, 741–772.
16. Wong, T.J.; Lim, F.J.; Gao, M.; Lee, G.H.; Ho, G.W. Photocatalytic H₂ production of composite one-dimensional TiO₂ nanostructures of different morphological structures and crystal phases with graphene. *Catal. Sci. Technol.* **2013**, *3*, 1086–1093.
17. Tsubota, T.; Ono, A.; Murakami, N.; Ohno, T. Characterization and photocatalytic performance of carbon nanotube material-modified TiO₂ synthesized by using the hot CVD process. *Appl. Catal. B* **2009**, *91*, 533–538.
18. Huang, Q.; Tian, S.; Zeng, D.; Wang, X.; Song, W.; Li, Y.; Xiao, W.; Xie, C. Enhanced photocatalytic activity of chemically bonded TiO₂/graphene composites based on the effective interfacial charge transfer through the C–Ti bond. *ACS Catal.* **2013**, *3*, 1477–1485.
19. Li, Y.; Li, L.; Li, C.; Chen, W.; Zeng, M. Carbon nanotube/titania composites prepared by a micro-emulsion method exhibiting improved photocatalytic activity. *Appl. Catal. A* **2012**, *427–428*, 1–7.
20. Ahmmad, B.; Kusumoto, Y.; Somekawa, S.; Ikeda, M. Carbon nanotubes synergistically enhance photocatalytic activity of TiO₂. *Catal. Commun.* **2008**, *9*, 1410–1413.
21. Ventosa, E.; Chen, P.; Schuhmann, W.; Xia, W. CNTs grown on oxygen-deficient anatase TiO_{2-δ} as high-rate composite electrode material for lithium ion batteries. *Electrochem. Commun.* **2012**, *25*, 132–135.
22. Chen, P.R.; Chew, L.M.; Xia, W. The influence of the residual growth catalyst in functionalized carbon nanotubes on supported Pt nanoparticles applied in selective olefin hydrogenation. *J. Catal.* **2013**, *307*, 84–93.
23. Becker, M.J.; Xia, W.; Tessonier, J.-P.; Blume, R.; Yao, L.; Schlögl, R.; Muhler, M. Optimizing the synthesis of cobalt-based catalysts for the selective growth of multiwalled carbon nanotubes under industrially relevant conditions. *Carbon* **2011**, *49*, 5253–5264.
24. Ventosa, E.; Xia, W.; Klink, S.; La Mantia, F.; Mei, B.; Muhler, M.; Schuhmann, W. Ammonia-annealed TiO₂ as a negative electrode material in Li-ion batteries: N doping or oxygen deficiency? *Chem. Eur. J.* **2013**, *19*, 14194–14199.
25. Xia, W.; Su, D.; Birkner, A.; Ruppel, L.; Wang, Y.; Wöll, C.; Qian, J.; Liang, C.; Marginean, G.; Brandl, W.; Muhler, M. Chemical vapor deposition and synthesis on carbon nanofibers: sintering of ferrocene-derived supported iron nanoparticles and the catalytic growth of secondary carbon nanofibers. *Chem. Mater.* **2005**, *17*, 5737–5742.
26. Kundu, S.; Nagaiah, T.C.; Chen, X.X.; Xia, W.; Bron, M.; Schuhmann, W.; Muhler, M. Synthesis of an improved hierarchical carbon-fiber composite as a catalyst support for platinum and its application in electrocatalysis. *Carbon* **2012**, *50*, 4534–4542.
27. Sánchez, M.D.; Chen, P.; Reinecke, T.; Muhler, M.; Xia, W. The role of oxygen- and nitrogen-containing surface groups on the sintering of iron nanoparticles on carbon nanotubes in different atmospheres. *ChemCatChem* **2012**, *4*, 1997–2004.
28. Santato, C.; Ulmann, M.; Augustynski, J. Photoelectrochemical properties of nanostructured tungsten trioxide films. *J. Phys. Chem. B* **2001**, *105*, 936–940.

29. Busser, G.W.; Mei, B.; Muhler, M. Optimizing the deposition of hydrogen evolution sites on suspended semiconductor particles using on-line photocatalytic reforming of aqueous methanol solutions. *ChemSusChem* **2012**, *5*, 2200–2206.
30. Ohtani, B.; Iwai, K.; Nishimoto, S.; Sato, S. Role of Platinum Deposits on Titanium(IV) Oxide Particles: Structural and Kinetic Analyses of Photocatalytic Reaction in Aqueous Alcohol and Amino Acid Solutions. *J. Phys. Chem. B* **1997**, *101*, 3349–3359.
31. Kowalska, E.; Mahaney, O.O.; Abe, R.; Ohtani, B. Visible-light-induced photocatalysis through surface plasmon excitation of gold on titania surfaces. *Phys. Chem. Chem. Phys* **2010**, *12*, 2344–2355.
32. Woan, K.; Pyrgiotakis, G.; Sigmund, W. Photocatalytic carbon-nanotube-TiO₂ composites. *Adv. Mater.* **2009**, *21*, 2233–2239.
33. Chen, T.; Feng, Z.; Wu, G.; Shi, J.; Ma, G.; Ying, P.; Li, C. Mechanistic studies of photocatalytic reaction of methanol for hydrogen production on Pt/TiO₂ by *in situ* Fourier transform IR and time-Resolved IR spectroscopy. *J. Phys. Chem. C* **2007**, *111*, 8005–8014.
34. Yu, J.G.; Xiang, Q.J.; Zhou, M.H. Preparation, characterization and visible-light-driven photocatalytic activity of Fe-doped titania nanorods and first-principles study for electronic structures. *Appl. Catal. B* **2009**, *90*, 595–602.
35. Dholam, R.; Patel, N.; Adami, M.; Miotello, A. Hydrogen production by photocatalytic water-splitting using Cr- or Fe-doped TiO₂ composite thin films photocatalyst. *Int. J. Hydrogen Energy* **2009**, *34*, 5337–5346.
36. Tatarchuk, B. Physical characterization of Fe/TiO₂ model supported catalysts I. Electron microscopic studies of reduction behavior. *J. Catal.* **1981**, *70*, 308–322.
37. Pumera, M. Carbon nanotubes contain residual metal catalyst nanoparticles even after washing with nitric acid at elevated temperature because these metal nanoparticles are sheathed by several graphene sheets. *Langmuir* **2007**, *23*, 6453–6458.
38. Tessonier, J.P.; Rosenthal, D.; Hansen, T.W.; Hess, C.; Schuster, M.E.; Blume, R.; Girgsdies, F.; Pfander, N.; Timpe, O.; Su, D.S.; Schlögl, R. Analysis of the structure and chemical properties of some commercial carbon nanostructures. *Carbon* **2009**, *47*, 1779–1798.
39. Lascovich, J.C.; Giorgi, R.; Scaglione, S. Evaluation of the sp²/sp³ ratio in amorphous carbon structure by XPS and XAES. *Appl. Surf. Sci.* **1991**, *47*, 17–21.
40. Veziri, C.M.; Pilatos, G.; Karanikolos, G.N.; Labropoulos, A.; Kordatos, K.; Kasselouri-Rigopoulou, V.; Kanellopoulos, N.K. Growth and optimization of carbon nanotubes in activated carbon by catalytic chemical vapor deposition. *Micro. Mesopor. Mater.* **2008**, *110*, 41–50.
41. Yang, J.; Wang, D.; Han, H.; Li, C. Roles of cocatalysts in photocatalysis and photoelectrocatalysis. *Acc. Chem. Res.* **2013**, *46*, 1900–1909.
42. Bledowski, M.; Wang, L.; Ramakrishnan, A.; Betard, A.; Khavryuchenko, O.V.; Beranek, R. Visible-light photooxidation of water to oxygen at hybrid TiO₂-polyheptazine photoanodes with photodeposited Co-Pi (CoO_x) cocatalyst. *Chemphyschem* **2012**, *13*, 3018–3024.